



ePlace-3D: Electrostatics based Placement for 3D-ICs

Jingwei Lu
Cadence Design Systems, Inc.
francesco.ljw@gmail.com

Hao Zhuang
Dept. CSE of UCSD
hao.zhuang@cs.ucsd.edu

Ilgweon Kang
Dept. CSE of UCSD
igkang@ucsd.edu

Pengwen Chen
Dept. Applied Maths of NCHU
pengwen@nchu.edu.tw

Chung-Kuan Cheng
Dept. CSE of UCSD
ckcheng@ucsd.edu

ABSTRACT

We propose a flat, analytic, mixed-size placement algorithm *ePlace-3D* for three-dimension integrated circuits (3D-ICs) using nonlinear optimization. Our contributions are (1) electrostatics based 3D density function with globally uniform smoothness (2) 3D numerical solution with improved spectral formulation (3) 3D nonlinear pre-conditioner for convergence acceleration (4) interleaved 2D-3D placement for efficiency enhancement. Our placer outperforms the leading work mPL6-3D and NTUplace3-3D with 6.44% and 37.15% shorter wirelength, 9.11% and 10.27% fewer 3D vertical interconnects (VI) on average of IBM-PLACE circuits. Validation on the large-scale modern mixed-size (MMS) 3D circuits shows high performance and scalability.

1. INTRODUCTION

Placement remains dominant on the overall quality of physical design automation [29, 30]. Based on logic synthesis [31], back-end design on timing [45], power [9, 44], routability [8, 38], variability [3, 42] etc. are highly impacted by placement performance. The emerging 3D-IC [28] challenges the traditional 2D placers [1, 2, 5, 17, 19, 25, 41] to produce 3D circuit layout with minimum wirelength yet limited vertical interconnects (through-silicon vias (TSVs), monolithic inter-tier vias (MIVs), etc.). Innovations of mixed-size 3D-IC placement become quite desirable.

Previous **combinatorial** 3D-IC placers form two categories. Folding based methods [4] folds the 2D-IC placement layout to produce 3D solution with local refinement. Partitioning based approaches [7, 18] minimize the usage of vertical resources. Kim et al. [18] partitions the netlist followed by tier assignment, then applies 2D quadratic placement [40] simultaneously over all the tiers. **Analytic** placers achieve better 3D-IC placement performance versus combinatorial algorithms. Goplen et al. [6] models the 3D-IC placement by a quadratic framework [5]. Hsu et al. [10] extends the 2D-IC placement prototype [11] and uses Bell-shape function [34] to smooth the vertical dimension. Luo et al. [27] utilizes the

2D algorithm in [1] and relaxes the discrete tiers via Huber function [12]. However, these modeling functions are only locally smooth. Moreover, their hierarchical cell clustering and grid coarsening would degrade the quality [25]. Separately, prior 3D placement benchmarks [13, 15] are of up to only 210K cells, which are too small to represent modern design complexity. Large-scale bookshelf 3D-IC placement benchmarks become desirable.

In this work, we extend the 2D placers ePlace [22, 23, 25] and ePlace-MS [22, 26] to the 3D domain. Our algorithm is named **ePlace-3D** and focused on **wirelength minimization** and **density equalization**, while other 3D-IC objectives like thermal are not covered. To the best of our knowledge, this is the first work in literature achieving analytically **global smoothness** along all the three dimensions. In contrast, previous analytic works [10, 27] only ensure (partially) local smoothness in their density functions [12, 34], while their less continuous cell movement would slow down placement convergence and cause more penalty on wirelength. We conduct analytic global placement and stochastic legalization in the entire 3D cuboid domain, which maximizes the search space thus further boost the solution quality. ePlace-3D well demonstrates the applicability of the electrostatic density model **eDensity** [23, 24] in various physical dimensions. Our specific contributions are listed as follows.

- **eDensity-3D**: an electrostatics based 3D density function ensuring global smoothness.
- A 3D numerical solution based on fast Fourier transform (FFT) and improved spectral formulation.
- A nonlinear 3D preconditioner to equalize all the moving objects in the optimization perspective.
- Interleaving coarse-grained 3D placement with fine-grained 2D placement to enhance efficiency.
- Our mixed-size 3D-IC placement prototype **ePlace-3D** outperforms the leading placers mPL6-3D [27] and NTUplace3-3D [10] with 6.44% and 37.15% shorter wirelength, 9.11% and 10.27% fewer 3D vertical interconnects, while runs 2.55 \times and 0.30 \times faster on average of all the ten IBM-PLACE benchmarks [13],

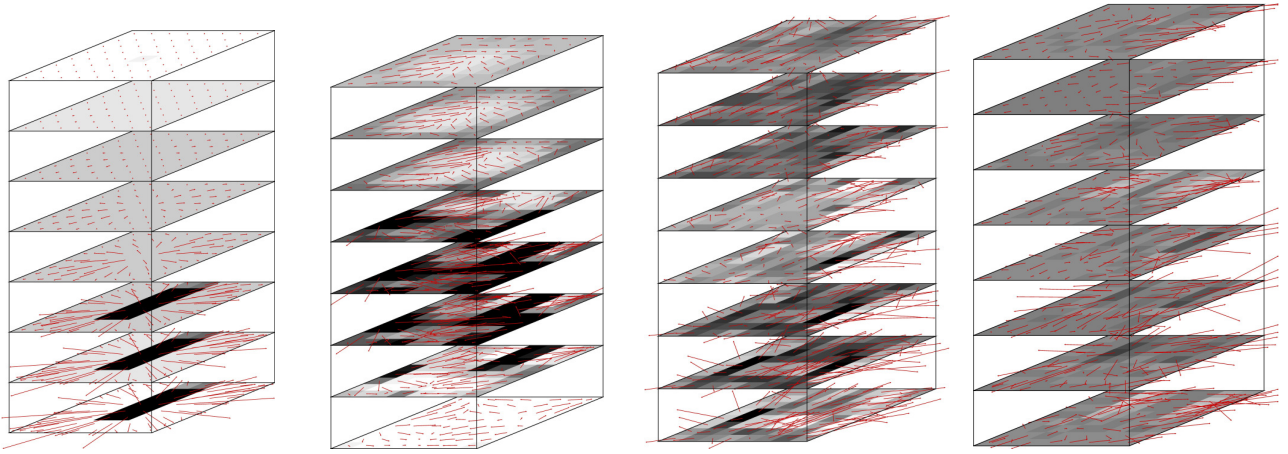
The remainder is organized as follows. Section 2 introduces the background knowledge. Section 3 discusses our 3D placement density function eDensity-3D, numerical solution, and nonlinear precondition. Section 4 provides an overview of ePlace-3D algorithm. Experiments and results are shown in Section 5. We conclude in Section 6.

Permission to make digital or hard copies of all or part of this work for personal or classroom use is granted without fee provided that copies are not made or distributed for profit or commercial advantage and that copies bear this notice and the full citation on the first page. Copyrights for components of this work owned by others than ACM must be honored. Abstracting with credit is permitted. To copy otherwise, or republish, to post on servers or to redistribute to lists, requires prior specific permission and/or a fee. Request permissions from permissions@acm.org.

ISPD '16, April 3–6, 2016, Santa Rosa, California, USA.

© 2016 ACM. ISBN 978-1-4503-4039-7/16/04...\$15.00

DOI: <http://dx.doi.org/10.1145/2872334.2872361>



(a) Iter=0, $U=6.18e17$, $\tau = 90.13\%$. (b) Iter=3, $U=5.84e16$, $\tau = 47.56\%$. (c) Iter=6, $U=3.56e15$, $\tau = 11.75\%$. (d) Iter=20, $U=2.07e14$, $\tau = 2.53\%$.

Figure 1: Iterative density-driven global placement (wirelength force disabled) with potential U and density overflow τ on the MMS ADAPTEC1 benchmark with three tiers and resolution of $8 \times 8 \times 8$. Electric density and field are shown by gray scale and red arrows. All the movable objects are initialized at the bottom tier where all IO blocks locate. eDensity-3D iteratively spreads all the movable objects evenly within the entire 3D domain to equalize the placement density.

2. BACKGROUND

Given a set V of n objects, net set N and 3D cuboid core region $R = [0, d_x] \times [0, d_y] \times [0, d_z]$, global placement is formulated as constrained optimization. The **constraint** desires all the objects to be accommodated with zero overlap. Let \mathbf{v} denote the placement solution, which consists of the physical coordinates of all the objects. The region R is uniformly decomposed into $m_x \times m_y \times m_z$ 3D bins denoted as set B . For every bin $b \in B$, the density $\rho_b(\mathbf{v})$ should not exceed the target density ρ_t . The **objective** is to minimize the total half-perimeter wirelength (HPWL) of all the nets. Let $HPWL_{e_x} = \max_{i,j \in e} |x_i - x_j|$ denote the horizontal wirelength of net e (similar for $HPWL_{e_y}$), the total 2D HPWL is $HPWL(\mathbf{v}) = \sum_{e \in N} (\beta_x HPWL_{e_x}(\mathbf{v}) + \beta_y HPWL_{e_y}(\mathbf{v}))$. We use β_x , β_y and β_z as dimensional weighting factors. 3D-IC placement needs **vertical interconnects**, such as through-silicon via (TSV) and monolithic inter-tier via (MIV), to penetrate silicon tiers. Diverse types of connects have different physical and electrical properties. However, ePlace-3D is compatible with any types of connects, which can be reflected on the weight of β_z . *In the remainder of this manuscript, we name all types of 3D vertical interconnects uniformly as VI for simplicity. The number of vertical interconnect units (#VI) is computed as how many times silicon tiers have been penetrated, e.g., one vertical connect between tier one and tier three is counted as two VI.* The nonlinear placement optimization is formulated as

$$\min_{\mathbf{v}} (HPWL(\mathbf{v}) + \beta_z \#VI) \text{ s.t. } \rho_b(\mathbf{v}) \leq \rho_t, \forall b \in B. \quad (1)$$

Analytic methods conduct placement using gradient-directed optimization. As $HPWL(\mathbf{v})$ is not differentiable, we use **wirelength smoothing** by weighted-average (WA) model [10].

$$W_{e_x}(\mathbf{v}) = \frac{\sum_{i \in e} x_i \exp(x_i/\gamma_x)}{\sum_{i \in e} \exp(x_i/\gamma_x)} - \frac{\sum_{i \in e} x_i \exp(-x_i/\gamma_x)}{\sum_{i \in e} \exp(-x_i/\gamma_x)} \quad (2)$$

Here $W_e(\mathbf{v}) = \beta_x W_{e_x}(\mathbf{v}) + \beta_y W_{e_y}(\mathbf{v}) + \beta_z W_{e_z}(\mathbf{v})$ and $W(\mathbf{v}) = \sum_e W_e(\mathbf{v})$. γ_x , γ_y and γ_z control the modeling accuracy.

Density function relaxes all the $|B|$ constraints in Eq. (1). Most 2D and 3D **quadratic** placers [6,18,19] follow the linear density force formulation by [5]. **Nonlinear** placers [1, 10,11,27] have their dedicated density functions. NTUplace3-3D [10] leverages bell-shape curve [34] for local smoothness in 3D domain. mPL6-3D [1] uses Helmholtz function to globally smoothen the 2D plane and Huber's function to locally smoothen the vertical dimension. The **electrostatics** based density function [25] converts objects to charges. By the Lorentz law, the electric repulsive force spreads charges away towards the electrostatic equilibrium state, which produces a globally even density distribution. Let $U(\mathbf{v})$ denote the density cost function, the constraints in Eq. (1) can be relaxed by the penalty factor λ , while the unconstrained optimization is shown as below.

$$\min_{\mathbf{v}} f(\mathbf{v}) = W(\mathbf{v}) + \lambda U(\mathbf{v}), \quad (3)$$

In this work, we set vertical connects as zero-volumed thus do not consider them in eDensity-3D¹. Therefore, the optimization of electrostatics will not be affected and can be still achieved based on the movement of netlist objects. **Density overflow** is used to terminate global placement and denoted as τ , which is

$$\tau = \frac{\sum_{b \in B} \max(V_b^m - \rho_t V_b^{WS}, 0)}{V_m}. \quad (4)$$

Here V_m is the total volume of all the movable objects, V_b^m is the total volume of objects in the bin b , and V_b^{WS} is the total whitespace in bin b . The volume of each cell is computed as its planar area multiplied by the depth of each tier.

¹Practically, vertical connects can never be zero volumed. However, for academic research we are able to simplify the engineering problems to boost scientific innovations. Similarly, state-of-the-art 2D placement academic works [1,2,17, 19,25,40,41] target wirelength only and ignore other objectives like timing, power and routability. As vertical connects may be of large volume thus significantly contribute to the placement density, we will put it in our future work.

3. EDENSITY-3D: 3D DENSITY FUNCTION

In this section, we introduce our novel 3D density function **eDensity-3D**, a fast numerical solution by spectral methods, and approximated 3D nonlinear preconditioner. The key insight is, we treat the third dimension equally as the other two dimensions, such that vertical cell movement will be as smooth as the planar movement in 2D placement. The behavior of eDensity-3D is visualized in Figure 1.

3.1 3D Density Function

Extending the planar function eDensity in [25], eDensity-3D models the entire placement instance as a 3D electrostatic field. Every placement object (standard cells, macros and fillers) is converted to a positively charged cuboid. The electric repulsive force spreads all the objects away from the high-density region. The 3D density cost U is modeled as the total potential energy of the system and defined as below

$$U(\mathbf{v}) = \sum_{i \in V} U_i(\mathbf{v}) = \sum_{i \in V} q_i \Phi_i(\mathbf{v}). \quad (5)$$

q_i denotes the electric quantity of the charge i and is set as the physical volume of placement object i . Φ_i is the electric potential at charge i . Charges with high potential will reduce the placement overlap by moving towards the direction of largest energy descent. Unlike the spatial density distribution $\rho(x, y, z)$ (Figure 1) which is coarse and non-differentiable, the electric potential distribution $\Phi(x, y, z)$ is globally smooth. We use the potential gradient (thus electric field), $\nabla \Phi(x, y, z) = \mathbf{E}(x, y, z)$, to direct cell movement for density equalization. Given a placement layout \mathbf{v} , we generate the density map $\rho(x, y, z)$, then compute the potential map $\Phi(x, y, z)$ by solving the **3D Poisson's equation**

$$\begin{cases} \nabla \cdot \nabla \Phi(x, y, z) = -\rho(x, y, z), \\ \hat{\mathbf{n}} \cdot \nabla \Phi(x, y, z) = 0, (x, y, z) \in \partial R, \\ \iiint_R \Phi(x, y, z) = \iiint_R \rho(x, y, z) = 0. \end{cases} \quad (6)$$

Here $\hat{\mathbf{n}}$ is the outer unit normal of the placement cube R . ∂R is the boundary and consists of orthogonal rectangular planes to enclose the placement cuboid. In Eq. (6), the first equation has $\nabla \cdot \nabla \equiv \frac{\partial^2}{\partial x^2} + \frac{\partial^2}{\partial y^2} + \frac{\partial^2}{\partial z^2}$. Neumann condition by the second equation requires that when any object i reaches any boundary plane, its density force vector will have the component perpendicular to the plane reduced to zero, in order to prevent i from penetrating the plane. The third equation shows that the integral of density $\rho(x, y, z)$ and potential $\Phi(x, y, z)$ within R are set to zero to ensure that (1) electric force drives all the charges towards even density distribution rather than pushing them to infinity, which matches the placement objective (2) the 3D Poisson's equation would have a unique solution by satisfying the Neumann condition. We differentiate the potential Φ_i on each charge i to generate the electric field $\nabla \Phi_i = \mathbf{E}_i = (E_{i_x}, E_{i_y}, E_{i_z})$. The electric (density) force is $\nabla U_i = q_i \nabla \Phi_i = q_i \mathbf{E}_i$.

3.2 3D Numerical Solution

Based on the 2D solution in [25], we solve the 3D Poisson's equation by spectral methods using frequency decomposition [39]. To satisfy the Neumann condition of zero gradients at the boundaries, we use sinusoidal wave to express the electric field $\mathbf{E}(x, y, z)$. We construct an odd and periodic field distribution by negatively mirroring itself w.r.t. the origin, then periodically extending it towards positive

and negative infinities. Electric potential and density distributions are then expressed by cosine waveforms, which are the integration and differentiation of the field. Let $a_{j,k,l}$ denote the 3D coefficients of the density frequency.

$$a_{j,k,l} = \frac{1}{n^3} \sum_{x,y,z} \rho(x, y, z) \cos(w_j x) \cos(w_k y) \cos(w_l z) \quad (7)$$

eDensity [25] sets $w_j = \pi \frac{j}{m_x}$, which equals the discrete index for the j th frequency component. However, as we are conducting placement in a continuous domain, the multiplication of x and w_j induces inconsistency. In this work, we propose **improved spectral methods** for the 3D placement density function. Specifically, we set $w_j = \pi \frac{j}{d_x}$ since x ranges within $(0, d_x)$. As a result, $w_j x = \pi j \frac{x}{d_x}$ well matches the original unit of discrete frequency index, and we have all the frequency indexes defined as $\{w_j, w_k, w_l\} = \{\frac{\pi j}{d_x}, \frac{\pi k}{d_y}, \frac{\pi l}{d_z}\}$. As mentioned in Section 2, here d_x, d_y and d_z represent the dimensions of the cuboid placement core region. $d_{\{x,y,z\}}$ can be set as any value since $w_{\{j,k,l\}}$ will be normalized by $\frac{\{x,y,z\}}{d_{\{x,y,z\}}}$. j, k and l range in $[0, n-1]$, which is only half of a cosine function period. In contrast, one complete function period centered at the origin is $[-n, n-1]$. Therefore, we have π rather than 2π in the above frequency index. We set $a_{0,0,0} = 0$ to remove the zero-frequency component. The spatial density distribution $\rho(x, y, z)$ is

$$\rho(x, y, z) = \sum_{j,k,l} a_{j,k,l} \cos(w_j x) \cos(w_k y) \cos(w_l z). \quad (8)$$

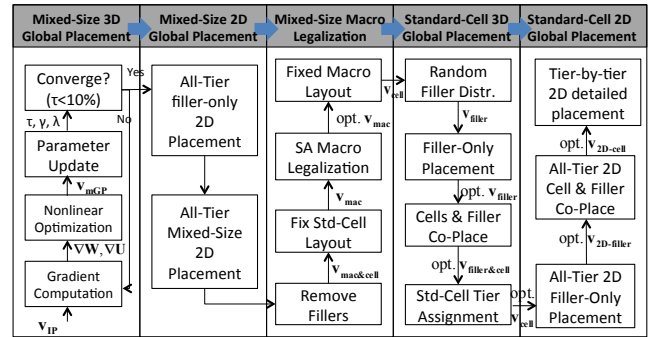


Figure 2: the flowchart of ePlace-3d.

To achieve $\nabla \cdot \nabla \Phi(x, y, z) = -\rho(x, y, z)$, the solution to the potential can be expressed as

$$\Phi(x, y, z) = \sum_{j,k,l} \frac{a_{j,k,l}}{w_j^2 + w_k^2 + w_l^2} \cos(w_j x) \cos(w_k y) \cos(w_l z). \quad (9)$$

By differentiating Eq. (9), we have the electric field distribution $\mathbf{E}(x, y, z) = (E_x, E_y, E_z)$ shown as below

$$\begin{cases} E_x(x, y, z) = \sum_{j,k,l} \frac{a_{j,k,l} w_j}{w_j^2 + w_k^2 + w_l^2} \sin(w_j x) \cos(w_k y) \cos(w_l z), \\ E_y(x, y, z) = \sum_{j,k,l} \frac{a_{j,k,l} w_k}{w_j^2 + w_k^2 + w_l^2} \cos(w_j x) \sin(w_k y) \cos(w_l z), \\ E_z(x, y, z) = \sum_{j,k,l} \frac{a_{j,k,l} w_l}{w_j^2 + w_k^2 + w_l^2} \cos(w_j x) \cos(w_k y) \sin(w_l z). \end{cases} \quad (10)$$

Let $|B| = m_x \times m_y \times m_z$ denote the total number of bins in global placement. Instead of quadratic complexity, above spectral equations can be efficiently solved using FFT algorithms [36] with $O(|B| \log |B|)$ complexity.

3.3 3D Nonlinear Precondition

Theoretically, preconditioning improves convergence rate rather than solution quality. However, as placement is a highly nonlinear, non-convex and ill-conditioned problem, the Hessian matrix with improved condition number would reshape the search direction for the nonlinear solver to follow. As a result, preconditioning would open the gate for unexplored high-dimension search space, while surprising quality enhancement would be expectable.

Preconditioned mixed-size placement should tolerate the huge physical and topological differences between all the standard cells, macros, and dummy fillers. In [25], the nonlinear preconditioner H for 2D placement is modeled as

$$H_{i_x} = \frac{\partial^2 f}{\partial x_i^2} = \frac{\partial^2 W}{\partial x_i^2} + \lambda \frac{\partial^2 U}{\partial x_i^2} \approx |N_i| + \lambda A_i. \quad (11)$$

Here N_i are all the nets incident to the object i , A_i is the 2D area of the object i . In 3D placement, we use V_i to denote the volume of i instead. The preconditioned gradient $\nabla f_{pre} = H^{-1} \nabla f$ then improves and accelerates the placement. Our studies show that Eq. (11) relies on the assumption of $\frac{\partial^2 W / \partial x_i^2}{\partial^2 U / \partial x_i^2} \approx \frac{|N_i|}{A_i}$. However, the third dimension weakens $\frac{\partial^2 W}{\partial x_i^2}$ and breaks the above assumption. As a result, $|N_i|$ dominates λV_i and makes fillers and macros with small $|N_i|$ spread faster than standard cells, as Eq. (12) shows

$$\|H_{i_x}^{-1} \nabla U\| = \left\| \frac{\partial U / \partial x_i}{\lambda V_i} \right\| \gg \left\| \frac{\partial f / \partial x_i}{|N_i| + \lambda V_i} \right\| = \|H_{i_x}^{-1} \nabla f\|. \quad (12)$$

Instead, we propose a new preconditioner as below

$$H_{i_x} = \frac{\partial^2 f}{\partial x_i^2} \approx \lambda \frac{\partial^2 U}{\partial x_i^2} \approx \lambda V_i, \quad (13)$$

The noise factors introduced by $|N_i|$ is resolved, where all the objects are being equalized in the optimizer's perspective and simultaneously spread over the entire domain. Experiments show that our 3D preconditioner reduces the global placement iterations by 15% and improves the wirelength by 30% over all the 16 MMS benchmarks.

3.4 Complexity

Complexity significantly impacts the placement runtime. In each iteration, we traverse all the bins to reset their density in $O(|B|)$ time, then traverse all the placement objects in $O(n)$ time to update the superimposed density map. By Eq. (7), (9) and (10), five times of 3D FFT computation are invoked, which costs $O(5n \log n)$ time. By our grid sizing strategy in Eq. (14), $|B|/n$ is limited to constant. The overall complexity is thus $O(|B| + n + 5n \log n) \approx O(n \log n)$.

In ePlace-3D, the placement domain is geometrically transformed from $R = [0, d_x] \times [0, d_y] \times [0, d_z]$ to $R' = [0, 1] \times [0, 1] \times [0, 1]$. We set the density resolutions $m_x = m_y = m_z = m_{3D}$ to make the placement domain R' uniformly decomposed into $|B| = m_{3D}^3$ cubic bins. Let V_R denote the total volume of R and $V_{C_{avg}}$ denote the average area of all standard cells. The grid sizing is set as

$$|B| = \frac{V_R}{k \times V_{C_{avg}} \times \rho_t^{-1}}. \quad (14)$$

Here every k standard cells are accommodated by one bin. Placement quality (efficiency) is determined by the value of k . In this work, we constantly set $k = 1.0$.

4. EPLACE-3D: OVERVIEW

ePlace-3D is built upon the infrastructure of ePlace-MS [26]. Figure 2 shows the flowchart of our algorithm. Given a placement instance, our algorithm minimizes the quadratic wirelength over the 3D domain to produce the initial solution \mathbf{v}_{IP} . To approach the optimum solution in the end, we make \mathbf{v}_{IP} as minimum-wirelength violation-tolerant.

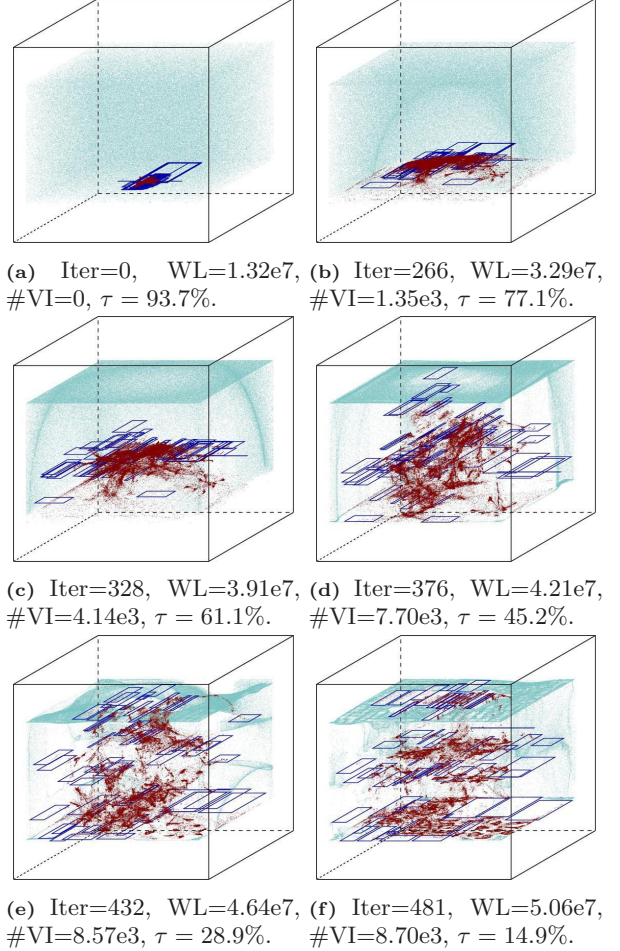


Figure 3: 3D-IC mixed-size global placement on MMS ADAPTEC1 with three tiers. Standard cells, macros and fillers are denoted by red dots, blue rectangles and cyan dots.

Our 3D-IC global placement is visualized in Figure 3. Unconnected fillers [1, 25] are inserted to populate up extra whitespace. All the fillers are equally sized by the average dimensions of all the standard cells. *The optimum solution of 3D global placement will have all the cells, macros and fillers orient towards discrete tiers.* Otherwise, some cuboid placement sites will be partially wasted, degrading the solution quality. Figure 3(f) illustrates the beauty of our approach, i.e., the analytic 3D placer is visually approaching density evenness from the vertical dimension, which ensures *negligible quality overhead during tier assignment.* We use Nesterov's method [35] as the nonlinear solver and determine the steplength by [25].

A multi-tier 2D-IC mixed-size global placement follows by assigning all the macros and standard cells to the closest

tiers and separately filling the remaining whitespace on each tier with fillers. Planar placement is conducted simultaneously over all the tiers. As wirelength smoothing is homogeneous over all the tiers (with the same γ), heterogeneous grid sizing is not feasible as density force is dependent on resolution by Eq. (10). We set all the tiers with the same density resolution m_{2D} , which is the maximum of that of all the tiers by Eq. (14) with $k = 1$. In practice, we have $O(m_{2D}^2) \approx O(m_{3D}^3)$. Figure 4 illustrates the progression.

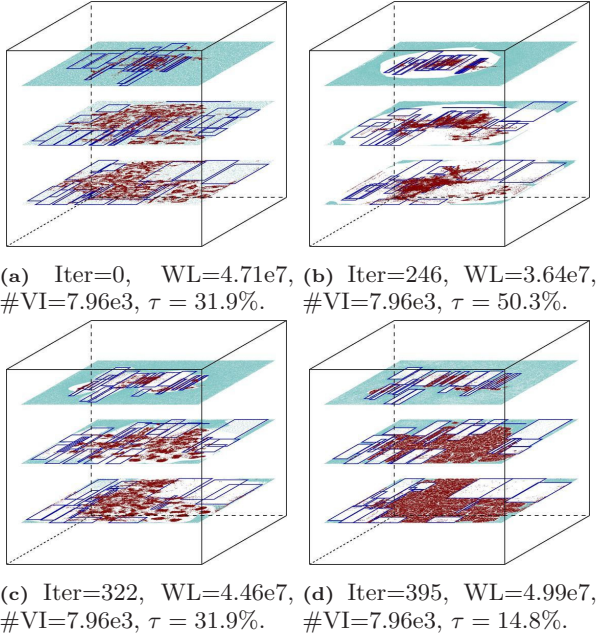


Figure 4: 2D-IC mixed-size global placement on MMS ADAPTEC1 with three tiers. Initial and final overflow are both larger than the final overflow of 3D placement due to finer granularity ($m_{2D} \gg m_{3D}$).

Our 3D-IC macro legalizer generates a legal macro layout with zero macro overlap and small wirelength overhead. The algorithm is stochastic based on simulated annealing [20]. A 3D-IC standard-cell global placement follows to mitigate the quality loss due to sub-optimal macro legalization. We assign standard cells to their closest tiers and conduct simultaneous 2D-IC standard-cell placement on all the tiers. The standard-cell layouts of all the tiers are locally refined. Figure 5 shows the respective placement progressions, more details can be found in [26]. The detailed placer from [37] is then invoked for a tier-by-tier standard-cell legalization and detailed placement from the bottom to the top tier.

In general, we have fine-grained 2D placement interleaved with coarse-grained 3D placement, which achieves a good trade-off between quality and efficiency. On average of all the ten IBM-PLACE circuits, the application of 2D refinement reduces the wirelength by more than 4%.

5. EXPERIMENTS AND RESULTS

We implement ePlace-3D using C programming language in the single-thread mode and execute the program in a Linux machine with Intel i7 920 2.67GHz CPU and 12GB memory. There is no benchmark specific parameter tuning in our work. #VI are controlled by the weighting factor β_z based on capacitance ratio. By [16], one TSV (VI) has

the capacitance of $C_{VI} = 30fF$ at 45nm tech-node. ITRS annual reports [14] show that unit capacitance of interconnects at intermediate routing layers is constantly $2pF/cm$ across various tech-nodes. Placement row height is $1.4\mu m$ at 45nm tech-node ($70nm$ M1 half-pitch, ten M1 tracks per row), capacitance becomes $C_{ROW} = 0.3fF$ for 2D interconnect spanning one-row height. Based on the length units for each benchmark, as well as our geometric transformation of the placement core region to be $[0, 1] \times [0, 1] \times [0, 1]$ as discussed in Section 3.4, we compute the respective capacitance ratio of one VI versus one unit wirelength and use it as the VI weight. Specifically, we have

$$\beta_z = \frac{\#tiers \times C_{VI}}{\#rows \times C_{ROW}} \quad (15)$$

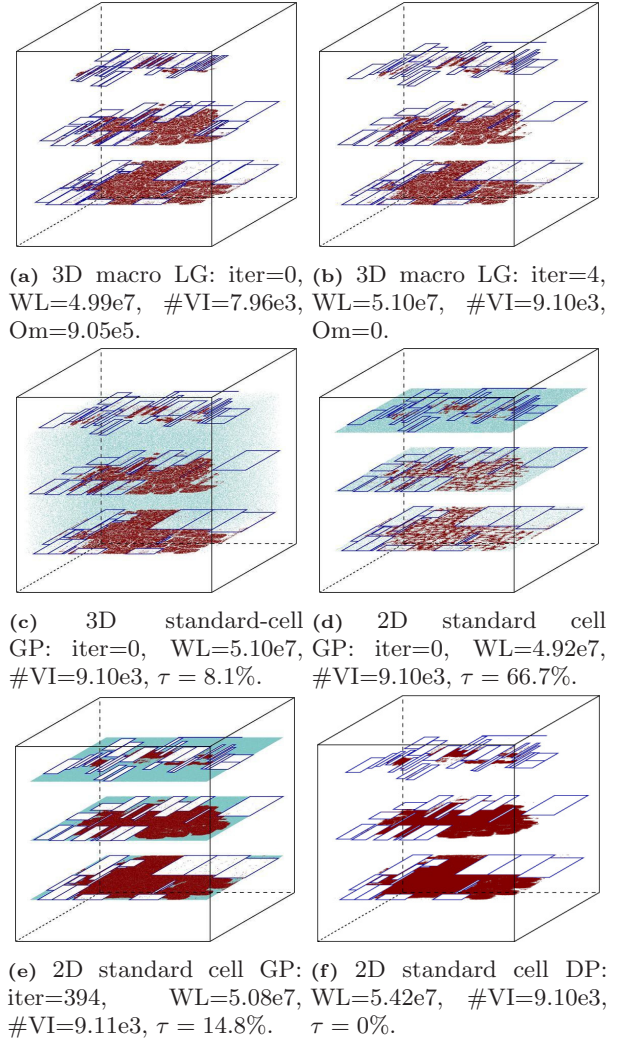


Figure 5: Post-placement on MMS ADAPTEC1 with three tiers. Standard cells, macros and fillers are denoted by red dots, blue rectangles and cyan dots. Om denotes the total macro overlap.

Notice that the focus of this work is the algorithm framework of 3D placement, not the accurate weight modeling of vertical connects. The weighting factor can be adjusted by VLSI designers for their particular needs, e.g., vertical

Table 1: HPWL (e7), #VI (vertical interconnect) (e3) and runtime (minutes) on the IBM-PLACE benchmark suite [13]. Cited results are marked with *. All the experiments are conducted under single-thread mode. The results are evaluated by the same scripts and normalized to ePlace-3D. The best result for each case is in bold-face.

| Categories | | | NTUplace3-3D [10] | | | mPL6-3D* [27] | | | ePlace-3D | | |
|------------|---------|--------|-------------------|-------------|-------|---------------|-------------|-------|-------------|-------------|-------|
| Benchmarks | # Cells | # Nets | HPWL | #VI | CPU | HPWL | #VI | CPU | HPWL | #VI | CPU |
| IBM01 | 12K | 12K | 0.34 | 0.69 | 0.20 | 0.26 | 1.04 | 2.95 | 0.25 | 1.31 | 0.58 |
| IBM03 | 22K | 22K | 0.76 | 3.32 | 0.50 | 0.59 | 3.11 | 4.72 | 0.56 | 3.27 | 1.33 |
| IBM04 | 27K | 26K | 1.00 | 2.60 | 0.60 | 0.81 | 2.95 | 6.41 | 0.74 | 3.53 | 1.88 |
| IBM06 | 32K | 33K | 1.30 | 3.99 | 0.80 | 1.05 | 3.97 | 6.20 | 0.92 | 4.50 | 2.98 |
| IBM07 | 45K | 44K | 1.92 | 5.73 | 1.30 | 1.59 | 4.68 | 8.64 | 1.50 | 4.39 | 3.87 |
| IBM08 | 51K | 48K | 2.08 | 4.90 | 1.70 | 1.71 | 3.94 | 11.23 | 1.54 | 4.90 | 4.75 |
| IBM09 | 52K | 50K | 1.92 | 3.88 | 1.50 | 1.45 | 3.24 | 14.61 | 1.40 | 3.18 | 5.63 |
| IBM13 | 82K | 84K | 3.69 | 3.98 | 2.60 | 2.88 | 5.59 | 19.62 | 2.67 | 4.73 | 8.65 |
| IBM15 | 158K | 161K | 9.16 | 15.67 | 7.20 | 6.79 | 10.52 | 46.82 | 6.39 | 9.16 | 40.25 |
| IBM18 | 210K | 201K | 13.41 | 12.19 | 13.60 | 9.16 | 15.22 | 52.09 | 9.47 | 6.83 | 63.07 |
| Avg. | 69K | 68K | 37.15% | 10.27% | 0.30× | 6.44% | 9.11% | 2.55× | 0.00% | 0.00% | 1.00× |

connects of different electric and physical attributes (TSVs, MIVs, super contacts, etc.).

We conduct experiments on IBM-PLACE [13] standard-cell benchmarks without macros or blockages, all of which are derived from real IC design. We include two state-of-the-art 3D-IC placers, mPL6-3D [27]², and NTUplace3-3D [10], in our experiments on IBM-PLACE. As other categories of algorithms (e.g., folding and partition based approaches) have been outperformed by analytic placement in literature, we do not include them in our experiments. We have obtained the binary of NTUplace3-3D from the original authors and executed it on our machine for experiments³. mPL6-3D is not available (as notified by the author), so we cite the performance from their latest publication [27]. We use exactly the same benchmark transformation as that by mPL6-3D and NTUplace3-3D. I.e., we insert four silicon tiers into each benchmark, scale down each tier to $\frac{1}{4}$ of the original 2D placement area, add 10% whitespace to each tier, and keep the aspect ratio of each tier to be the same as the original 2D design. As a result, all the experiments on the three placers, including those from [27], are conducted on exactly the same **IBM-PLACE-3D** benchmarks. As HPWL and #VI are being computed in exactly the same way, the performance comparison among the three placers are fair. The results on IBM-PLACE cases are shown in Table 1. On average of all the ten circuits, ePlace-3D outperforms mPL6-3D and NTUplace3-3D with 6.44% and 37.15% shorter wirelength together with 9.11% and 10.27% fewer VIs. ePlace-3D runs 2.55× faster than mPL6-3D but 0.30× slower than NTUplace3-3D, nevertheless, the improvement on wirelength (37.15%) and VI (10.27%) is significant.

To validate the scalability of ePlace-3D, we also conduct experiments on the large-scale **modern mixed-size (MMS)** benchmarks [43] with on average 829K and up to 2.5M netlist objects. MMS benchmarks was first published in DAC 2009. The circuits inherit the same netlists and den-

sity constraints ρ_t from ISPD 2005 [33] and ISPD 2006 [32] benchmarks but have all the macros freed to place. The original planar placement domain is geometrically transformed to be of 2, 3 and 4 silicon tiers, each tier is equally downsized to keep both the aspect ratio and total silicon area unchanged. All the standard cells and macros keep their original dimensions and span only one tier. MMS circuits have all their fixed objects with zero area (volume) and outside the placement boundaries, and we geometrically transform them to the boundary of the bottom (first) tier. Also, as macros are all free to move, we skip the geometrical transformation of the fixed macro layout from 2D to 3D, which is sub-optimal and usually causes quality loss. Similar to mPL6-3D [27] and NTUplace3-3D [10], we add 10% extra whitespace to each tier, in order to relieve the placement dilemma due to the increased area ratio between large macros and silicon tiers⁴. There are benchmark-dependent target density ρ_t for eight out of the sixteen MMS circuits. Detailed circuit statistics can be found in Table 1 of [43]. We create evaluation scripts to compute the total wirelength, number of vertical interconnects, and legality of the produced 3D-IC placement solution. The results on the MMS benchmarks are shown in Table 2. Notice that here HPWL is the original half-perimeter wirelength. It is not penalized by the amount of density overflow, since the density overflow in 3D domain is of one more dimension thus hard to compare with that of 2D domain. The binary of NTUplace3-3D does not work with these benchmarks, while the binary of mPL6-3D is not available for use. As a result, we compare the 3D MMS placement solutions with the best published (golden) 2D results in literature [26]. By using two, three and four tiers, ePlace-3D outperforms the golden 2D placement with on average 13.67%, 20.50% and 27.54% shorter wirelength. On the other side, the average ratio between the number of vertical interconnect units versus the number of placement objects (standard cells and macros) are only 2.17%, 4.30% and 6.10%, respectively. These vertical connect ratios are much smaller than the average VI ratio on IBM-PLACE, which are more than 9% for all the three placers in Table 1.

²Although mPL6-3D has extension to thermal-aware placement, its experiments on the IBM-PLACE cases are based on their original prototype driven by only wirelength and density but not thermal.

³There is a small quality gap on NTUplace3-3D between our local experiment results and that published in [10], which may be due to the differences in computing platforms.

⁴BIGBLUE3, NEWBLUE2 and NEWBLUE3 have very large macros. For the tier insertion of two, three and four, we add 20%, 30% and 40% whitespace to each tier to make sure that the largest macro can be accommodated.

Table 2: HPWL (e6), #VI (vertical interconnect) and runtime (mins) on MMS circuits. Cited results are marked with *. All the experiments are in single-thread mode. The HPWL and CPU results are normalized to the best published 2D placement results [26], #VI are normalized to # objects.

| Benchmarks | # tiers | | ePlace-MS* [26] | | ePlace-3D w/ 2 tiers | | | ePlace-3D w/ 3 tiers | | | ePlace-3D w/ 4 tiers | | |
|------------|---------|--------|-----------------|--------|----------------------|-------|--------|----------------------|-------|--------|----------------------|--------|--------|
| | # Objs | # Nets | HPWL | CPU | HPWL | #VI | CPU | HPWL | #VI | CPU | HPWL | #VI | CPU |
| ADAPTEC1 | 211K | 221K | 67.15 | 5.47 | 59.51 | 5733 | 24.63 | 54.19 | 9104 | 14.65 | 51.3 | 13568 | 16.03 |
| ADAPTEC2 | 255K | 266K | 77.37 | 7.43 | 73.97 | 9269 | 39.67 | 75.38 | 9929 | 25.18 | 59.97 | 18085 | 24.57 |
| ADAPTEC3 | 451K | 466K | 164.50 | 27.23 | 141.97 | 5557 | 95.48 | 136.85 | 18203 | 88.55 | 120.29 | 28694 | 94.42 |
| ADAPTEC4 | 496K | 515K | 148.38 | 29.35 | 126.94 | 8149 | 107.15 | 113.22 | 13811 | 121.40 | 106.34 | 14527 | 118.13 |
| BIGBLUE1 | 278K | 284K | 86.82 | 7.82 | 76.06 | 8272 | 40.63 | 71.34 | 10508 | 36.17 | 63.64 | 19403 | 38.05 |
| BIGBLUE2 | 557K | 577K | 130.18 | 13.70 | 109.27 | 2565 | 70.25 | 97.1 | 5347 | 63.58 | 90.14 | 9241 | 64.95 |
| BIGBLUE3 | 1096K | 1123K | 302.29 | 72.98 | 251.77 | 24466 | 268.47 | 271.27 | 42053 | 291.38 | 295.38 | 62669 | 388.08 |
| BIGBLUE4 | 2177K | 2229K | 657.92 | 204.15 | 577.98 | 21263 | 491.97 | 537.2 | 50552 | 563.98 | 500.25 | 113590 | 420.17 |
| ADAPTEC5 | 843K | 867K | 310.54 | 48.35 | 258.18 | 22705 | 170.90 | 244.57 | 27764 | 146.22 | 223.44 | 50732 | 149.22 |
| NEWBLUE1 | 330K | 338K | 61.85 | 10.87 | 56.36 | 5901 | 28.15 | 53.05 | 7295 | 24.08 | 48.85 | 12346 | 25.07 |
| NEWBLUE2 | 441K | 465K | 162.93 | 62.40 | 179.82 | 25571 | 67.27 | 143.5 | 43642 | 77.20 | 169.78 | 53487 | 72.98 |
| NEWBLUE3 | 494K | 552K | 304.15 | 17.53 | 240.47 | 7686 | 308.62 | 365.10 | 48979 | 410.73 | 397.46 | 51597 | 265.67 |
| NEWBLUE4 | 646K | 637K | 228.54 | 29.73 | 197.21 | 11372 | 110.02 | 177.82 | 29767 | 112.80 | 171.21 | 35067 | 101.78 |
| NEWBLUE5 | 1233K | 1284K | 392.27 | 63.40 | 344.95 | 45995 | 202.12 | 303.05 | 64336 | 195.52 | 280.42 | 95768 | 216.22 |
| NEWBLUE6 | 1255K | 1288K | 408.36 | 69.65 | 379.59 | 10901 | 222.72 | 325.35 | 50487 | 194.57 | 298.82 | 66983 | 180.88 |
| NEWBLUE7 | 2507K | 2636K | 894.31 | 191.47 | 814.79 | 18615 | 363.30 | 696.27 | 92943 | 375.65 | 670.51 | 111562 | 353.92 |
| Avg. | 829K | 859K | 0.00% | 1.00× | 13.67% | 2.17% | 3.13× | 20.50% | 4.30% | 3.03× | 27.54% | 6.10% | 2.94× |

Due to the introduction of the third dimension, the search space of placement optimization is substantially enlarged. However, the runtime increase is just 3×, which indicates high efficiency of ePlace-3D.

We also study the trends of HPWL and #VI by linearly sweeping the number of tiers and exponentially sweeping the VI weight. We select eight out of the sixteen MMS benchmarks (ADAPTEC1, ADAPTEC4, BIGBLUE1, BIGBLUE2, BIGBLUE3, BIGBLUE4, NEWBLUE6, NEWBLUE7), all of which could accommodate the maximum macro block after inserting ten tiers. Keeping the same aspect ratio, the area of each tier is scaled down by ten times with the insertion of 10% extra whitespace. Figure 6 shows that ePlace-3D is able to reduce the total 2D wirelength by up to 40% (with the insertion of up to ten tiers), while #VI is roughly scaled up by the number of tiers. VI weight sweeping is conducted

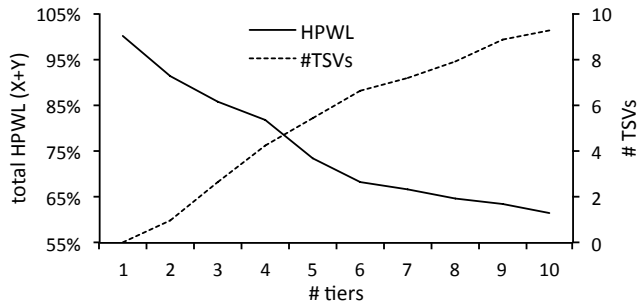


Figure 6: Avg. HPWL and #VI of eight selected MMS cases w.r.t. number of silicon tiers.

on all the sixteen MMS benchmarks. Figure 7 shows the trends of average HPWL and #VI by dividing the normal VI weight by up to 32 times (i.e. $\times 0.03125$). The total 2D HPWL saturates at the reduction of 7%, while #VI is scaled up by roughly 2.5×.

Our 3D-IC placement algorithm shows significant quality improvement while limited runtime overhead. BIGBLUE4 and NEWBLUE7 are the largest circuits with 2.2M and 2.5M cells, and they consume the longest runtime on the 3D-

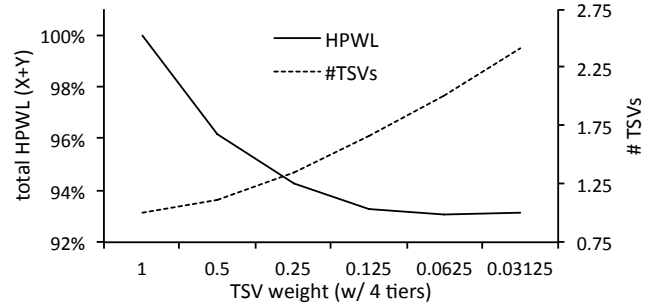


Figure 7: Avg. HPWL and #VI of all the sixteen MMS cases w.r.t. VI weights.

IC placement. However, compared to the respective golden 2D placement solutions, the runtime ratio is upper-bounded by 2.5×, which is still less than the average runtime ratios of 3.13× for two tiers, 3.03× for three tiers and 2.94× for four tiers, respectively. To this end, ePlace-3D shows good scalability and acceptable efficiency on the large cases.

In this work, we do not test ePlace-3D on circuits with fixed macros, as geometrically transforming the 2D floorplan into 3D is difficult and usually error-prone. However, ePlace-3D shows high performance and scalability on MMS benchmarks with lots of movable large macros, which is more difficult to place than fixed-macro layouts. As a result, we are confident on the performance of ePlace-3D on any circuits with fixed macros. The advantage of 3D tier insertion vanishes if there are large macros to accommodate (BIGBLUE3, NEWBLUE3, etc.). Transformation of 2D planar macros into 3D cuboid macros would resolve this issue and ensure the consistent benefits by inserting more tiers. However, it is beyond this work and will be covered in future.

6. CONCLUSION

We propose the first electrostatics based placement algorithm **ePlace-3D**, which is effective and efficient for 3D-ICs with uniform exploration over the entire 3D space. Our 3D-IC density function leverages the analogy between place-

ment spreading and electrostatic equilibrium, while global and uniform smoothness is realized at all the three dimensions. Our balancing and preconditioning techniques prevent solution oscillation or divergence. The interleaved 3D coarse-grained optimization followed by 2D fine-grained post processing obtains a good trade-off between quality and efficiency. The experimental results validate the high performance and scalability of our approach, indicating the benefits of placement smoothness. In future, we will develop 3D density function to address the volume of vertical interconnects (VI). We would also like to explore advanced technology for 3D-IC placement/routing with patterning and graph coloring technology [21].

7. ACKNOWLEDGMENT

The authors acknowledge (1) Prof. Dae Hyun Kim and Prof. Sung Kyu Lim for providing the 3D-IC flow scripts and IWLS testcases (2) Dr. Meng-Kai Hsu and Prof. Yao-Wen Chang for providing the binary of NTUplace3-3D (3) Dr. Guojie Luo and Prof. Jason Cong for providing the binary of mPL6-3D (4) the support of NSF CCF-1017864.

8. REFERENCES

- [1] T. F. Chan, J. Cong, J. R. Shinnerl, K. Sze, and M. Xie. mPL6: Enhanced Multilevel Mixed-Size Placement. In *ISPD*, pages 212–214, 2006.
- [2] T.-C. Chen, Z.-W. Jiang, T.-C. Hsu, H.-C. Chen, and Y.-W. Chang. NTUPlace3: An Analytical Placer for Large-Scale Mixed-Size Designs with Preplaced Blocks and Density Constraint. *IEEE TCAD*, 27(7):1228–1240, 2008.
- [3] Y.-G. Chen, T. Wang, K.-Y. Lai, W.-Y. Wen, Y. Shi, and S.-C. Chang. Critical Path Monitor Enabled Dynamic Voltage Scaling for Graceful Degradation in Sub-Threshold Designs. In *DAC*, pages 1–6, 2014.
- [4] J. Cong, G. Luo, J. Wei, and Y. Zhang. Thermal-Aware 3-D IC Placement Via Transformation. In *ASPDAC*, pages 780–785, 2007.
- [5] H. Eisenmann and F. M. Johannes. Generic Global Placement and Floorplanning. In *DAC*, pages 269–274, 1998.
- [6] B. Goplen and S. Sapatnekar. Efficient Thermal Placement of Standard Cells in 3D ICs using a Force Directed Approach. In *ICCAD*, 2003.
- [7] B. Goplen and S. Sapatnekar. Placement of 3-D ICs with Thermal and Interlayer Via Considerations. In *DAC*, pages 626–631, 2007.
- [8] S. K. Han, K. Jeong, A. B. Kahng, and J. Lu. Stability and Scalability in Global Routing. In *SLIP*, pages 1–6, 2011.
- [9] Q. He, D. Chen, and D. Jiao. From Layout Directly to Simulation: A First-Principle Guided Circuit Simulator of Linear Complexity and Its Efficient Parallelization. *IEEE CPMT*, 2(4):687–699, 2012.
- [10] M.-K. Hsu, V. Balabanov, and Y.-W. Chang. TSV-Aware Analytical Placement for 3D IC Designs Based on a Novel Weighted-Average Wirelength Model. *IEEE TCAD*, 32(4):497–509, 2013.
- [11] M.-K. Hsu and Y.-W. Chang. Unified Analytical Global Placement for Large-Scale Mixed-Size Circuit Designs. *IEEE TCAD*, 2012.
- [12] P. J. Huber. *Robust Statistics*. John Wiley and Sons, 1981.
- [13] IBM-PLACE. <http://er.cs.ucla.edu/benchmarks/ibm-place>. 2001.
- [14] ITRS. <http://www.itrs.net/Links/2012ITRS/Home2012.htm>. 2012.
- [15] IWLS. <http://iwls.org/iwls2005/benchmarks.html>. 2005.
- [16] M. Jung et al. How to Reduce Power in 3D IC Designs: A Case Study with OpenSPARC T2 Core. In *CICC*, 2013.
- [17] A. B. Kahng and Q. Wang. A Faster Implementation of APlace. In *ISPD*, pages 218–220, 2006.
- [18] D. H. Kim, K. Athikulwongse, and S. K. Lim. A Study of Through-Silicon-Via Impact on the 3-D Stacked IC Layout. In *ICCAD*, 2009.
- [19] M.-C. Kim and I. Markov. ComPLx: A Competitive Primal-dual Lagrange Optimization for Global Placement. In *DAC*, 2012.
- [20] S. Kirkpatrick, C. D. G. Jr., and M. P. Vecchi. Optimization by Simulated Annealing. *Science*, 220(4598):671–680, 1983.
- [21] W. Lin, M. McGrath, I. Ramzy, T. H. Lai, and D. Lee. Detecting Job Interference in Large Distributed Multi-Agent Systems - A Formal Approach. In *IEEE IM*, 2013.
- [22] J. Lu. *Analytic VLSI Placement using Electrostatic Analogy*. Ph.D. Dissertation, University of California, San Diego, 2014.
- [23] J. Lu, P. Chen, C.-C. Chang, L. Sha, D. Huang, C.-C. Teng, and C.-K. Cheng. ePlace: Electrostatics based Placement using Fast Fourier Transform and Nesterov’s Method. *ACM TODAES*, 20(2):article 17, 2015.
- [24] J. Lu, P. Chen, C.-C. Chang, L. Sha, D. J.-H. Huang, C.-C. Teng, and C.-K. Cheng. FFTPL: An Analytic Placement Algorithm Using Fast Fourier Transform for Density Equalization. In *ASICON*, pages 1–4, 2013.
- [25] J. Lu, P. Chen, C.-C. Chang, L. Sha, D. J.-H. Huang, C.-C. Teng, and C.-K. Cheng. ePlace: Electrostatics based Placement using Nesterov’s Method. In *DAC*, pages 1–6, 2014.
- [26] J. Lu, H. Zhuang, P. Chen, H. Chang, C.-C. Chang, Y.-C. Wong, L. Sha, D. Huang, Y. Luo, C.-C. Teng, and C.-K. Cheng. ePlace-MS: Electrostatics based Placement for Mixed-Size Circuits. *IEEE TCAD*, 34(5):685–698, 2015.
- [27] G. Luo, Y. Shi, and J. Cong. An Analytical Placement Framework for 3-D ICs and Its Extension on Thermal Awareness. *IEEE TCAD*, 2013.
- [28] P.-W. Luo, T. Wang, C.-L. Wey, L.-C. Cheng, B.-L. Sheu, and Y. Shi. Reliable Power Delivery System Design for Three-Dimensional Integrated Circuits (3D ICs). In *ISVLSI*, pages 356–361, 2012.
- [29] I. L. Markov, J. Hu, and M.-C. Kim. Progress and Challenges in VLSI Placement Research. In *DAC*, 2012.
- [30] J. Miao, A. Gerstlauer, and M. Orshansky. Approximate Logic Synthesis under General Error Magnitude and Frequency Constraints. In *ICCAD*, pages 779–786, 2013.
- [31] J. Miao, A. Gerstlauer, and M. Orshansky. Multi-Level Approximate Logic Synthesis under General Error Constraints. In *ICCAD*, pages 504–510, 2014.
- [32] G.-J. Nam. ISPD 2006 Placement Contest: Benchmark Suite and Results. In *ISPD*, pages 167–167, 2006.
- [33] G.-J. Nam et al. The ISPD2005 Placement Contest and Benchmark Suite. In *ISPD*, pages 216–220, 2005.
- [34] W. C. Naylor, R. Donnelly, and L. Sha. Non-Linear Optimization System and Method for Wire Length and Delay Optimization for an Automatic Electric Circuit Placer. In *US Patent 6301693*, 2001.
- [35] Y. E. Nesterov. A Method of Solving A Convex Programming Problem with Convergence Rate $O(1/k^2)$. *Soviet Math*, 27(2):372–376, 1983.
- [36] T. Oura. General Purpose FFT Package, <http://www.kurims.kyoto-u.ac.jp/~oura/fft.html>. 2001.
- [37] M. Pan, N. Viswanathan, and C. Chu. An Efficient and Effective Detailed Placement Algorithm. In *ICCAD*, pages 48–55, 2005.
- [38] C.-W. Sham, E. F.-Y. Young, and J. Lu. Congestion Prediction in Early Stages of Physical Design. *ACM TODAES*, 14(1):12:1–18, 2009.
- [39] G. Skollermo. A Fourier Method for the Numerical Solution of Poisson’s Equation. *Mathematics of Computation*, 29(131):697–711, 1975.
- [40] P. Spindler, U. Schlichtmann, and F. M. Johannes. Kraftwerk2 - A Fast Force-Directed Quadratic Placement Approach Using an Accurate Net Model. *IEEE TCAD*, 27(8):1398–1411, 2008.
- [41] N. Viswanathan, M. Pan, and C. Chu. FastPlace3.0: A Fast Multilevel Quadratic Placement Algorithm with Placement Congestion Control. In *ASPDAC*, pages 135–140, 2007.
- [42] T. Wang, C. Zhang, J. Xiong, and Y. Shi. Eagle-Eye: A Near-Optimal Statistical Framework for Noise Sensor Placement. In *ICCAD*, pages 437–443, 2013.
- [43] J. Z. Yan, N. Viswanathan, and C. Chu. Handling Complexities in Modern Large-Scale Mixed-Size Placement. In *DAC*, 2009.
- [44] X. Zhang, J. Lu, Y. Liu, and C.-K. Cheng. Worst-Case Noise Area Prediction of On-Chip Power Distribution Network. In *SLIP*, pages 1–8, 2014.
- [45] H. Zhuang, J. Lu, K. Samadi, Y. Du, and C.-K. Cheng. Performance-Driven Placement for Design of Rotation and Right Arithmetic Shifters in Monolithic 3D ICs. In *ICCCAS*, pages 509–513, 2013.